

Enhanced valley splitting in monolayer WSe₂ due to magnetic exchange field

Chuan Zhao¹, Tenzin Norden¹, Peiyao Zhang¹, Puqin Zhao^{1,2}, Yingchun Cheng², Fan Sun¹, James P. Parry¹, Payam Taheri¹, Jieqiong Wang³, Yihang Yang⁴, Thomas Scrace¹, Kaifei Kang^{1,3}, Sen Yang³, Guo-xing Miao⁴, Renat Sabirianov⁵, George Kioseoglou⁶, Wei Huang², Athos Petrou¹ and Hao Zeng^{1,3*}

Exploiting the valley degree of freedom to store and manipulate information provides a novel paradigm for future electronics. A monolayer transition-metal dichalcogenide (TMDC) with a broken inversion symmetry possesses two degenerate yet inequivalent valleys^{1,2}, which offers unique opportunities for valley control through the helicity of light^{3–5}. Lifting the valley degeneracy by Zeeman splitting has been demonstrated recently, which may enable valley control by a magnetic field^{6–9}. However, the realized valley splitting is modest (~ 0.2 meV T⁻¹). Here we show greatly enhanced valley splitting in monolayer WSe₂, utilizing the interfacial magnetic exchange field (MEF) from a ferromagnetic EuS substrate. A valley splitting of 2.5 meV is demonstrated at 1 T by magnetoreflectance measurements and corresponds to an effective exchange field of ~ 12 T. Moreover, the splitting follows the magnetization of EuS, a hallmark of the MEF. Utilizing the MEF of a magnetic insulator can induce magnetic order and valley and spin polarization in TMDCs, which may enable valleytronic and quantum-computing applications^{10–12}.

TMDCs, such as MoS(Se)₂ and WS(Se)₂, are semiconducting graphite analogues composed of a layer of atoms covalently bonded, with stacks of these layers held together by van der Waals interactions^{13,14}. Monolayer TMDCs with a broken inversion symmetry possess two degenerate yet inequivalent valleys, related by time-reversal symmetry². This property and strong spin–orbit coupling is responsible for the unique physics of TMDCs, such as coupled spin and valley degrees of freedom¹. Together with a direct bandgap, TMDCs offer the opportunity to excite carriers selectively within a particular valley with a specific valley pseudospin using circularly polarized light^{3–5,15,16}. Furthermore, in electron- or hole-doped samples, valley Hall and spin Hall effects can be observed^{1,17,18}. Recently, spontaneously valley-polarized two-dimensional electron gas pockets have been observed in WS₂ monolayers¹⁹. Lifting the valley degeneracy in these materials is of great interest because it would allow the control of valley polarization for memory and logic applications^{17,20,21}. This has been achieved recently by applying an external magnetic field to Zeeman split the band edge states in different valleys^{7–9}. The valley splitting reported, however, is moderate at ~ 0.2 meV T⁻¹ (ref. 22). Another recent work reported g factors of up to 13 in the WSe₂ monolayer, or so-called narrow line emission centres²³. Although the mechanism remains to be understood, such small

splitting values make magnetic control only feasible at high fields and practical applications difficult. It has also been reported that valley degeneracy can be broken by intense circularly polarized light through the optical Stark effect^{24,25}.

An alternative approach to overcome the small valley-splitting issue is to utilize an interfacial MEF^{10,11}, which breaks the time-reversal symmetry. A giant and tunable valley splitting has been predicted theoretically in monolayer MoTe₂ on a EuO substrate^{10,11}. The exchange coupling between the ferromagnetic EuO and MoTe₂ can result in a valley splitting of 44 meV (ref. 11). Experimentally, EuS is among the few known magnetic insulators chosen to provide the MEF, because the large magnetic moment of Eu²⁺ ($S_z \approx 7 \mu_B$) and large exchange coupling ($J \approx 10$ meV) lead to a large MEF ($\propto JS_z$) (ref. 26). Some physics of the proximity effect in ferromagnetic/semiconductor hybrids has been discussed by Korenev, specifically the magnetic state in the ferromagnetic layer can be optically detected and manipulated²⁷. More recently, a substantial MEF of 14 T has been measured by the Zeeman spin Hall effect in graphene/EuS heterostructures²⁸. Proximity-induced ferromagnetism in graphene and topological insulators have also been reported^{29–31}.

In this work, we demonstrate experimentally greatly enhanced valley splitting in monolayer WSe₂ with an MEF induced by an EuS substrate. Its valley-specific optical interband transitions were measured by magnetoreflectance to probe the exciton valley splitting. The valley splitting of WSe₂/EuS samples has been enhanced by an order of magnitude to 2.5 meV at 1 T. More importantly, the field dependence of Zeeman splitting follows the field-dependent magnetization of EuS, a hallmark of exchange-field-induced Zeeman splitting. Our work shows that to harness the MEF from a ferromagnetic material is an effective approach for valley control and to induce valley/spin polarization in monolayer TMDCs, which can be superior to spin injection, which has potential difficulties such as pinholes and barrier breakdown.

Magnetoreflectance measurements were carried out in the Faraday geometry (Supplementary Schematic 4 in Supplementary Section I) on monolayer WSe₂ to determine their excitonic transitions and from these the valley splitting. The monolayer film consists of an ensemble of single-crystal triangles with a high density to achieve an adequate signal-to-noise ratio in reflectance measurements. In our study, we focused only on the lowest-energy ('A') exciton transitions. Figure 1a,b shows schematic diagrams of

¹Department of Physics, University at Buffalo, State University of New York, Buffalo, New York 14260, USA. ²Key Laboratory of Flexible Electronics and Institute of Advanced Materials, Jiangsu National Synergetic Innovation Center for Advanced Materials, Nanjing Technical University, Nanjing 211816, China.

³School of Science, MOE Key Laboratory of Nonequilibrium Synthesis and Modulation of Condensed Matter, Xi'an Jiaotong University, Xi'an 710049, China.

⁴Institute of Quantum Computing, University of Waterloo, Waterloo, Ontario, Canada. ⁵Department of Physics, University of Nebraska-Omaha, Omaha, Nebraska 68182, USA. ⁶Department of Material Science and Technology, University of Crete, Heraklion, GR 71003, Greece. *e-mail: haozeng@buffalo.edu

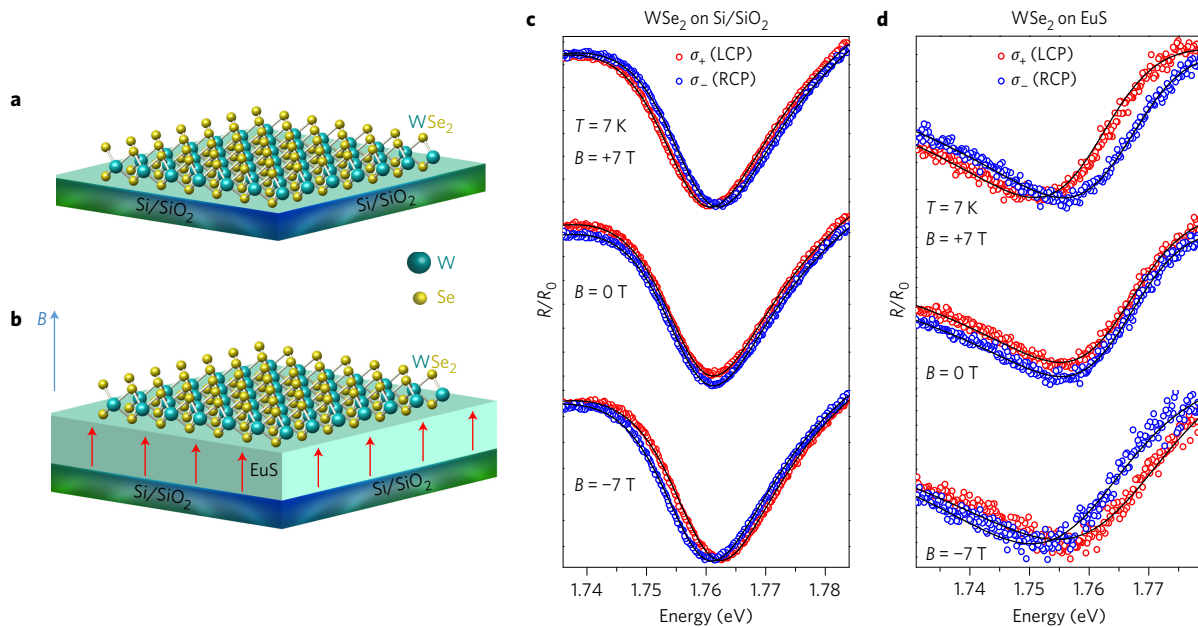


Figure 1 | Schematic diagrams of the WSe₂ monolayer on the substrates. a,b, The Si/SiO₂ substrate (a) and the ferromagnetic EuS substrate (b). The magnetic field is perpendicular to the plane. Reflectance spectra from the A exciton of monolayer WSe₂ recorded at $T = 7$ K. **c,d**, WSe₂ on the Si/SiO₂ substrate (c) and WSe₂ on the EuS substrate (d). Top, $B = +7$ T; middle, $B = 0$ T; bottom, $B = -7$ T. σ_+ (σ_-) corresponds to the transition at the K (K') valley. There is no splitting for spectra at $B = 0$, for either the Si/SiO₂ or the EuS substrate. At $+7$ T, the σ_+ (σ_-) component shifts to lower (higher) energy. At -7 T, the energy shift is in the opposite direction. By comparing c and d, it is clear that the energy splitting for WSe₂ on the EuS substrate is noticeably higher than that on the Si/SiO₂ substrate. The red circles (blue squares) indicate the σ_+ (σ_-) incident polarization. The dots are experimental data and solid lines are the fitting results using the 'absorptive and dispersive' line shape.

the WSe₂ monolayer on Si/SiO₂ and the ferromagnetic EuS substrates, respectively. The magnetic field is perpendicular to the plane. In Fig. 1c,d, we compare the reflectance spectra of monolayer WSe₂ on both the SiO₂ and EuS substrates, measured at 0 and ± 7 T, respectively, at 7 K. The vertical axis is the ratio R/R_0 , where R denotes the reflectance from WSe₂ and R_0 denotes the reflectance from the SiO₂ or EuS substrate adjacent to WSe₂. Taking the ratio of R/R_0 allows the removal of background signal from the substrates. The middle plot in Fig. 1c shows the zero-field reflectance signal from the A exciton of monolayer WSe₂ on SiO₂; left circularly polarized (LCP) light (σ_+) corresponds to the K and right circularly polarized (RCP) light (σ_-) corresponds to the K' valleys. The exciton features were fitted using a complex (absorptive plus dispersive) Fano line shape to extract the transition energies. A clear transition at 1.76 eV is observed at $B = 0$, which is consistent with a previously reported value for the A exciton of monolayer WSe₂ (ref. 32). As expected, the σ_+ and σ_- spectra match perfectly with each other, which indicates no energy splitting of the two valleys, as required by the time-reversal symmetry. Similarly, there is no measurable excitonic splitting at $B = 0$ for WSe₂ on EuS, as shown in the middle plot of Fig. 1d. On the application of a $+7$ T magnetic field, however, a clear valley splitting is observed for WSe₂ on SiO₂ (Fig. 1c, top). The σ_+ spectrum (A-exciton transition at the K valley) shifts to a lower energy, whereas the σ_- spectrum shifts to a higher energy. The valley splitting is defined as $\Delta E \equiv E(\sigma_-) - E(\sigma_+)$, where $E(\sigma_+)$ and $E(\sigma_-)$ refer to the fitted peak energy of σ_+ and σ_- , respectively. When a -7 T field is applied, the sign of the valley splitting is reversed, as shown in the lower plot of Fig. 1c; ΔE is 1.5 meV at 7 T, which is consistent with previously reported values^{7–9}. In WSe₂ on EuS, the valley splitting is equal to 3.9 meV at 7 T (Fig. 1d). This enhanced value implies that the valley splitting does not just come from the Zeeman effect caused by the external field; there is also an important contribution from the ferromagnetic EuS substrate. The reflectance spectra from the WSe₂/EuS sample are broader than those from WSe₂/SiO₂. The broadening primarily

results from the interactions between the WSe₂ layer and the EuS substrate, which cannot be removed by taking the ratio R/R_0 .

To elucidate the role of EuS, the field dependence of the valley Zeeman splitting, ΔE , measured at 7 K is shown in Fig. 2. For WSe₂ on a SiO₂ substrate, the field dependence is linear, with a slope of 0.20 meV T^{-1} , consistent with previously reported values^{9,22}. In contrast, ΔE for WSe₂ on an EuS substrate shows a pronounced nonlinear behaviour—it first increases rapidly with increasing field for $-1 \text{ T} < B < +1 \text{ T}$. For $|B| > 1 \text{ T}$, the slope decreases with increasing field and eventually reaches a constant value of 0.20 meV T^{-1} , very close to the slope for WSe₂ on a SiO₂ substrate. The slope for $-1 \text{ T} < B < +1 \text{ T}$, however, is 2.5 meV T^{-1} , which is an order of magnitude higher than the slope for WSe₂ on a SiO₂ substrate. The enhanced valley-splitting value in WSe₂/EuS suggests an effective exchange field of about 12 T at $B = 1 \text{ T}$, which possibly results from the interfacial MEF.

Below we discuss how spurious effects, particularly the contribution of the magnetic dipole field of EuS, are ruled out. We estimate the maximum dipole-field contribution from EuS to be 1.2 T (see the discussion below), which is an order of magnitude smaller than the exchange field. Thus, the dipole field of EuS cannot be a significant contributor to the enhanced valley splitting. Furthermore, if the enhanced valley splitting is, indeed, because of the interfacial exchange field, to insert a non-magnetic spacer layer between WSe₂ and EuS should interrupt the exchange coupling as a result of its short-range nature. To check this, we measured the valley splitting of WSe₂ on EuS with a 10 nm SiO₂ spacer inserted in between them. In Fig. 2b we plot the field-dependent valley splitting for the WSe₂/SiO₂ and WSe₂/SiO₂/EuS samples. As can be seen from Fig. 2b, there is no measurable difference between the behaviour of the exciton valley splittings of WSe₂ on EuS with the SiO₂ spacer and that of WSe₂ on the SiO₂ substrate. This clearly rules out the dipole field as the origin of the enhanced valley splitting because the stray field is not significantly reduced by the 10 nm spacer.

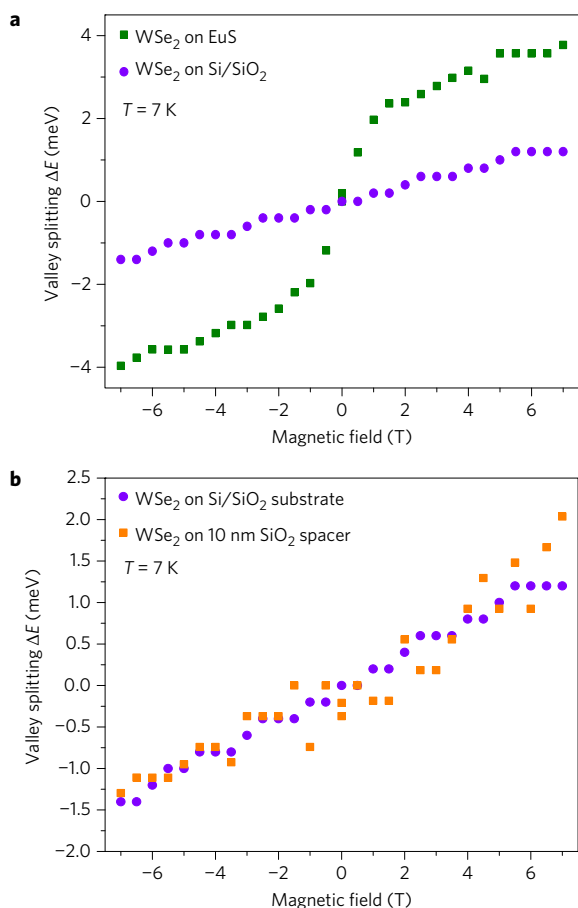


Figure 2 | Measured valley splitting ΔE as a function of magnetic field. **a**, WSe₂ on EuS versus SiO₂ substrates. Purple circles, Si/SiO₂ substrate; green squares, EuS substrate. On Si/SiO₂, with an increasing field ΔE increases linearly with a slope of 0.20 meV T⁻¹. On the EuS substrate, the splitting is greatly enhanced, with an initial slope of 2.5 meV T⁻¹ at $-1 \text{ T} < B < +1 \text{ T}$. At $|B| > 1 \text{ T}$, the slope gradually decreases to the value of WSe₂ on the Si/SiO₂ substrate. **b**, WSe₂ on SiO₂ (10 nm)/EuS versus SiO₂ substrates. Purple circles, Si/SiO₂; yellow squares, 10 nm SiO₂ spacer. Both show a linear field dependence with an identical slope of 0.20 meV T⁻¹.

The interfacial MEF should be proportional to the magnetization of the ferromagnetic substrate. To confirm unambiguously the origin of the enhanced valley splitting, systematic field and temperature dependences of the splitting were measured (Fig. 3a), and compared with the field-dependent magnetization of EuS measured at different temperatures (Fig. 3b). A linear background of 0.20 meV T⁻¹ is subtracted from all curves in Fig. 3a, and the net value is attributed to MEF and denoted as ΔE_{ex} . It can be seen that at 7, 12 and 20 K, ΔE_{ex} shows a nonlinear field dependence— at low fields, ΔE_{ex} increases rapidly with increasing field, starting from an initial value close to zero at $B = 0$. With the field increases further, the rate of increase of ΔE_{ex} slows down and then tends towards saturation at high fields. With increasing temperature, ΔE_{ex} decreases accordingly. Such behaviours are very similar to the field- and temperature-dependent magnetization of EuS, as shown in Fig. 3b. The measured saturation magnetization M_S of EuS at 7 K is 1,000 e.m.u. cm⁻³, slightly lower than the bulk M_S value of 1,200 e.m.u. cm⁻³ ($\sim 7 \mu_B$ per Eu²⁺) at 0 K. EuS has a cubic structure and is magnetically soft. The strong shape anisotropy of the 10 nm thin film forces the magnetic easy axis to lie in the plane. This explains the shape of the magnetization versus field loops with a very low remanent magnetization, and a relatively high saturation field ($\sim 1.2 \text{ T}$), which corresponds to the demagnetization field of $4\pi M_S$. Therefore, WSe₂ does not show a measurable spontaneous valley splitting even below the EuS Curie temperature (T_C) of 16.6 K. Similar behaviour is also observed in the electroluminescence polarization in spin light-emitting diodes with an Fe spin injector³³. ΔE_{ex} versus B shows nonlinear behaviour even at 20 K, above the expected T_C of EuS. This is also consistent with the temperature-dependent magnetization showing a tail well above 20 K (Supplementary Fig. 6). The magnitude of ΔE_{ex} at 7 T is comparable to the Zeeman splitting caused by the external field alone. At 50 K, the ΔE_{ex} value is greatly reduced and it increases with B essentially linearly with a slope of just 0.04 meV T⁻¹, as shown in Fig. 3a, as expected from the paramagnetic behaviour of EuS. The very similar field and temperature dependence shown in Fig. 3a,b suggests that ΔE_{ex} is directly correlated to the out-of-plane magnetization of EuS. To demonstrate further the correlation, Fig. 3c shows ΔE_{ex} versus B measured at different temperatures superimposed on magnetization, M versus B . Both ΔE_{ex} and M values are normalized by their respective saturated values at 7 K. Remarkably, the valley-exchange splitting ΔE_{ex} of WSe₂ measured

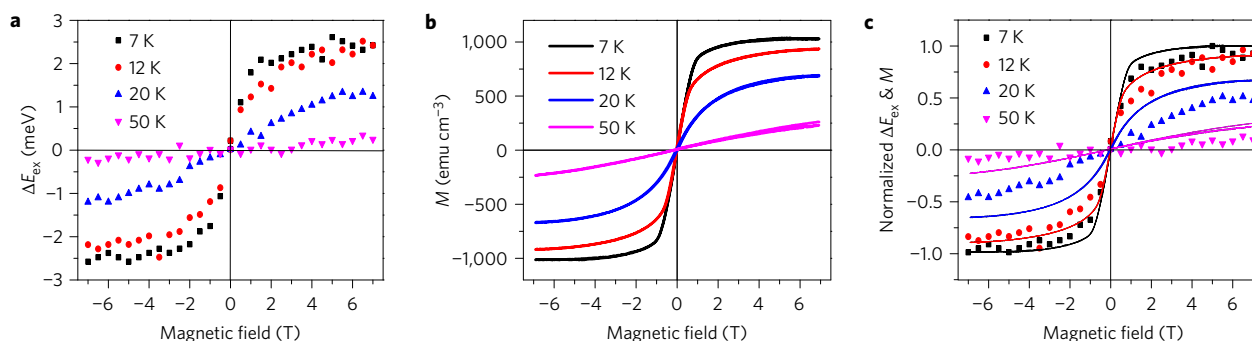


Figure 3 | Comparing the magnetic-field-dependent valley-exchange splitting of WSe₂/EuS and the field-dependent magnetization of EuS measured at different temperatures. **a**, Field-dependent valley-exchange splitting ΔE_{ex} due exclusively to MEF for WSe₂ measured at 7, 12, 20 and 50 K. A linear background of 0.20 meV T⁻¹, attributed to the Zeeman splitting caused by the external B field, is subtracted. ΔE_{ex} shows a nonlinear field dependence at 7 K (black squares), 12 K (red circles) and 20 K (blue triangles), but a linear field dependence at 50 K (purple triangles). **b**, Magnetization M of EuS as a function of the field measured at 7, 12, 20 and 50 K. The saturation magnetization at 7 K is 1,000 e.m.u. cm⁻³, slightly lower than the 1,200 e.m.u. cm⁻³ expected at 0 K. The similarity between M and ΔE_{ex} is apparent. **c**, Field-dependent ΔE_{ex} of WSe₂ and M of EuS superimposed on each other. Both ΔE_{ex} and M are normalized by their saturated values at 7 K. Points, normalized ΔE_{ex} ; lines, normalized M . It can be seen that they match with each other well at 7 and 12 K, which confirms unambiguously that the origin of the enhanced valley splitting is caused by the MEF. They show deviations from each other at higher temperatures, possibly because of a slight shift in sample position in the magnetoreflectance measurements.

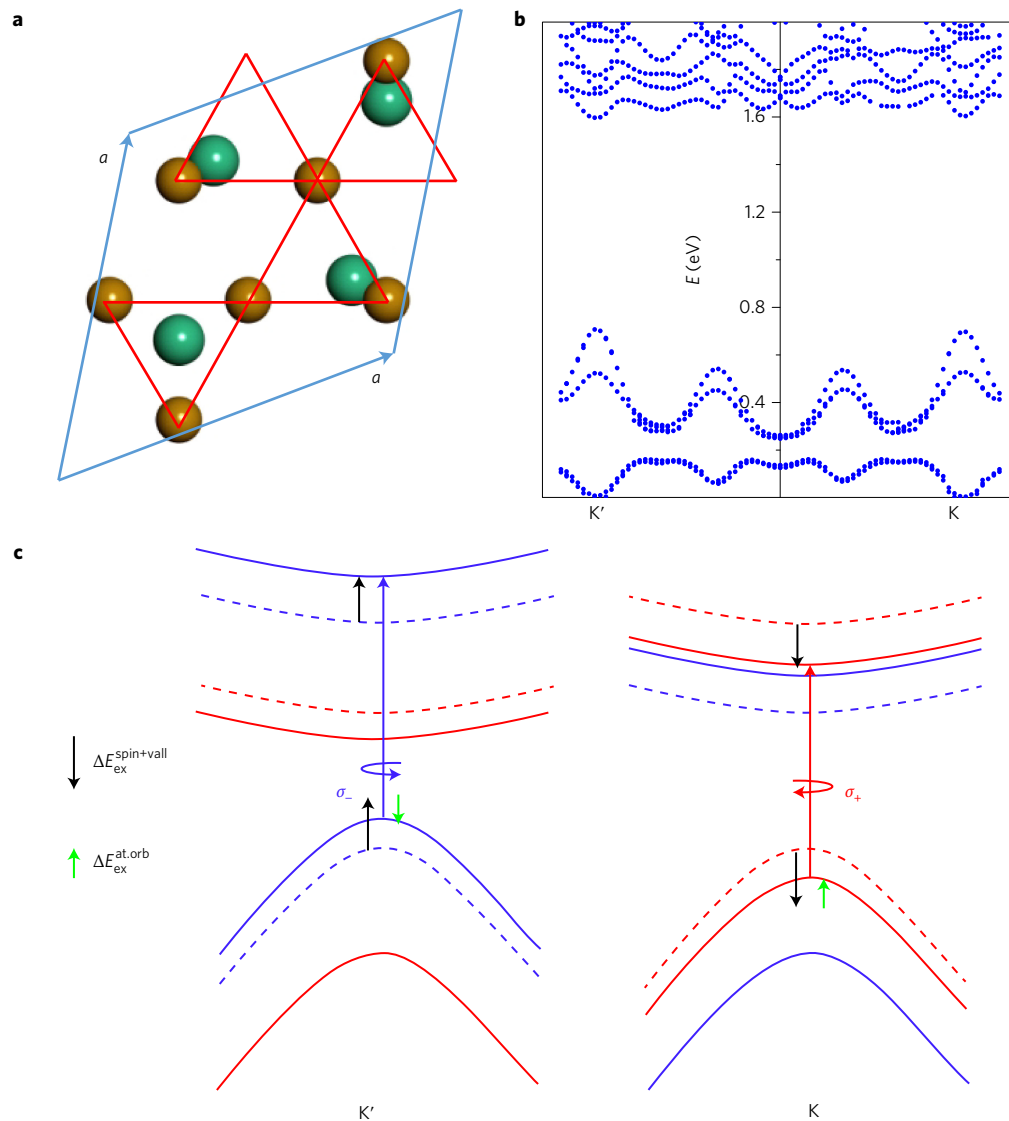


Figure 4 | Calculated band structure and valley-exchange splitting of WSe₂/EuS. **a**, Top view of the WSe₂/EuS interface used in the calculations. The lattice parameters of the selected unit cell of WSe₂ match closely those of EuS. Brown spheres represent W atoms and green spheres represent S atoms. **b**, The band structure of the WSe₂/EuS bilayer in the vicinity of the bandgap along the Γ -K and Γ -K' directions calculated by DFT. **c**, A schematic energy diagram at the K and K' valleys showing energy splitting of the bands in exchange-coupled WSe₂/EuS, and the corresponding A exciton transitions at the K and K' valleys. Red, spin-up bands; blue, spin-down bands; black arrows, net energy shift caused by spin and valley (spin+vall) orbital moment contributions; green arrows, energy shift caused by atomic orbital (at.orb) moment contributions. The valley exciton splitting originates mainly from the atomic orbital moment contributions. The spin moment contribution cannot be ruled out because of the different exchange coupling to the conduction and valence bands.

by magnetorefectance and the out-of-plane magnetization M of EuS measured by a vibrating-sample magnetometer (VSM) match with each other well for the measurement temperatures of 7 and 12 K. This shows unambiguously that the valley-exciton splitting in monolayer WSe₂ originates from the interfacial MEF, and thus scales with the magnetization of EuS. For higher temperatures, there is some noticeable deviation. Although the exact reason is not clear, we cannot rule out the possibility of a small shift of the sample spot as the temperature was raised.

We further investigated the valley-exchange splitting and magnitude of MEF using density functional theory (DFT) calculations of the band structure of a monolayer of WSe₂ deposited on an EuS(111) slab substrate. The system is shown schematically in Fig. 4a. There is a slight mismatch in lattice parameters of EuS and WSe₂ of about $\sim 3\%$ with the unit cell of $\mathbf{a}' = 3\mathbf{a} - \mathbf{b}$ (\mathbf{a} and \mathbf{b} are primitive lattice vectors of WSe₂). Figure 4b shows

the band structure of the WSe₂/EuS bilayer in the vicinity of the bandgap along the Γ -K and Γ -K' directions calculated by DFT. The direct optical bandgap occurs at the K (K') point. We focus now on the top valence and bottom conduction bands, as shown schematically in Fig. 4c. The top two valence bands in WSe₂ are spin split at the K point by ~ 0.46 eV because of the strong spin-orbit coupling on the W site. The highest valence band at the K point has spin-up character (red), whereas at K' it is spin down (blue). The opposite is true for the second-highest valence band because of the opposite spin of the electron in this band with respect to the top valence band. The conduction bands show a much smaller spin splitting (~ 0.041 eV) caused by the spin-orbit coupling. In the absence of a magnetic field, the energy of the top valence (bottom conduction) bands (shown by the dashed lines) at K and K' are degenerate because of the time-reversal symmetry, despite different spin characters.

The degeneracy is lifted, however, when WSe₂ is subjected to an external magnetic field or exchange field caused by the EuS substrate. Bands of opposite spin characters are shifted in opposite directions, that is, spin-up bands (red) are shifted downward and spin-down bands (blue) are shifted upward. The shifted bands are shown by the solid lines in Fig. 4c. With an external magnetic field, the energy-level shifts can be attributed to contributions from the spin, atomic orbital and valley orbital magnetic moments^{6–9}. The energy shifts caused by these different contributions are indicated by black and green arrows in Fig. 4c. The spin magnetic moment should not affect the optical transition as it shifts both conduction and valence bands by the same amount. The contribution of valley orbital magnetic moment is also negligible because of small differences in effective mass^{7,22}. The atomic orbital moment, on the other hand, differs for valence and conduction bands because the conduction band is mainly composed of a *d* orbital with a magnetic quantum number $m = 0$, whereas the valence band corresponds to *d* orbitals with $m = 2$ in K and $m = -2$ in K' valleys⁷. It does clearly contribute to the energy splitting of valley exciton transitions. In the presence of exchange fields, we expect the dominating contributions to the valley exciton splitting to be from the atomic orbital moment. However, a spin moment contribution may not be ruled out. Owing to the difference in the symmetry of the *d* orbitals, the Zeeman-like exchange contribution from the spin magnetic moment to the conduction and valence bands can be different. They are opposite in K and K' valleys, which can then contribute to the valley exciton splitting. As a result, the interband transition (*A* exciton) at the K valley for spin-up bands (σ_+) is $\Delta_{\text{opt}}^{\uparrow}(\text{K}) = E(\text{c}, \text{K}) - E(\text{v}, \text{K}) = 1.106 \text{ eV}$ versus that at the K' valley for spin-down bands (σ_-), $\Delta_{\text{opt}}^{\downarrow}(\text{K}') = E(\text{c}, \text{K}') - E(\text{v}, \text{K}') = 1.116 \text{ eV}$ (Supplementary Table I). The energy splitting for the *A* exciton at the K and K' valleys is thus about 10 meV, equivalent to an external magnetic field of about 50 T. As a result of the large magnitude of the MEF, EuS serves as a 'magnetic field amplifier' to enhance the valley exciton splitting.

The experimental splitting is a much smaller than the theoretically predicted value. This is not surprising considering that the EuS surface is modelled as an ideal Eu-terminated surface, whereas the experimentally prepared interface between WSe₂ and EuS is more complex. EuS grown by electron-beam evaporation is polycrystalline with only a fraction of the surface reconstructed (111) facets exposed. The other high-symmetry surfaces, such as (100) and (110), have lattice mismatch and considerably less Eu sites at the surface. However, it is clear that by optimizing the interface, there is great room to enhance the experimental valley splitting. By using a magnetic insulator with T_C above room temperature, such as yttrium iron garnet, it is also possible to realize enhanced valley splitting at room temperature, which is critical for device applications.

In conclusion, we have demonstrated a greatly enhanced valley exciton splitting in monolayer WSe₂ by utilizing the interfacial MEF from the ferromagnetic EuS substrate. The valley splitting is enhanced by more than an order of magnitude, equivalent to an effective magnetic field of 12 T. The field and temperature dependence of splitting scales with the magnetization of EuS, which confirms the exchange-field origin. Our work offers an enhanced capability to control the valley and spin polarization. For example, by electric gating, it is possible to tune the chemical potential to polarize selected valleys. As the charge carriers are also carriers of spin and valley-dependent orbital angular momentum, anomalous charge, spin and valley Hall effects are expected. The convenient manipulation of such degrees of freedom offers a new model for classical and quantum information-processing applications.

Methods

Methods and any associated references are available in the [online version of the paper](#).

Received 13 October 2016; accepted 14 March 2017;
published online 1 May 2017

References

- Xiao, D., Liu, G.-B., Feng, W., Xu, X. & Yao, W. Coupled spin and valley physics in monolayers of MoS₂ and other group-VI dichalcogenides. *Phys. Rev. Lett.* **108**, 196802 (2012).
- Zhu, Z., Cheng, Y. & Schwingenschlögl, U. Giant spin-orbit-induced spin splitting in two-dimensional transition-metal dichalcogenide semiconductors. *Phys. Rev. B* **84**, 153402 (2011).
- Cao, T. *et al.* Valley-selective circular dichroism of monolayer molybdenum disulphide. *Nat. Commun.* **3**, 887 (2012).
- Mak, K. F., He, K., Shan, J. & Heinz, T. F. Control of valley polarization in monolayer MoS₂ by optical helicity. *Nat. Nanotechnol.* **7**, 494–498 (2012).
- Zeng, H. L., Dai, J. F., Yao, W., Xiao, D. & Cui, X. D. Valley polarization in MoS₂ monolayers by optical pumping. *Nat. Nanotechnol.* **7**, 490–493 (2012).
- Li, Y. *et al.* Valley splitting and polarization by the Zeeman effect in monolayer MoSe₂. *Phys. Rev. Lett.* **113**, 266804 (2014).
- Aivazian, G. *et al.* Magnetic control of valley pseudospin in monolayer WSe₂. *Nat. Phys.* **11**, 148–152 (2015).
- MacNeill, D. *et al.* Breaking of valley degeneracy by magnetic field in monolayer MoSe₂. *Phys. Rev. Lett.* **114**, 037401 (2015).
- Srivastava, A. *et al.* Valley Zeeman effect in elementary optical excitations of monolayer WSe₂. *Nat. Phys.* **11**, 141–147 (2015).
- Zhang, Q. Y., Yang, S. Y. A., Mi, W. B., Cheng, Y. C. & Schwingenschlögl, U. Large spin-valley polarization in monolayer MoTe₂ on top of EuO(111). *Adv. Mater.* **28**, 959–966 (2016).
- Qi, J. S., Li, X., Niu, Q. & Feng, J. Giant and tunable valley degeneracy splitting in MoTe₂. *Phys. Rev. B* **92**, 121403 (2015).
- Rohling, N., Russ, M. & Burkard, G. Hybrid spin and valley quantum computing with singlet-triplet qubits. *Phys. Rev. Lett.* **113**, 176801 (2014).
- Matte, H. S. *et al.* MoS₂ and WS₂ analogues of graphene. *Angew. Chem. Int. Ed.* **49**, 4059–4062 (2010).
- Zhao, W. *et al.* Evolution of electronic structure in atomically thin sheets of WS₂ and WSe₂. *ACS Nano* **7**, 791–797 (2013).
- Yuan, H. T. *et al.* Generation and electric control of spin-valley-coupled circular photogalvanic current in WSe₂. *Nat. Nanotechnol.* **9**, 851–857 (2014).
- Eginligil, M. *et al.* Dichroic spin-valley photocurrent in monolayer molybdenum disulphide. *Nat. Commun.* **6**, 7636 (2015).
- Lee, J., Mak, K. F. & Shan, J. Electrical control of the valley Hall effect in bilayer MoS₂ transistors. *Nat. Nanotechnol.* **11**, 421–425 (2016).
- Mak, K. F., McGill, K. L., Park, J. & McEuen, P. L. The valley Hall effect in MoS₂ transistors. *Science* **344**, 1489–1492 (2014).
- Scrace, T. *et al.* Magnetoluminescence and valley polarized state of a two-dimensional electron gas in WS₂ monolayers. *Nat. Nanotechnol.* **10**, 603–607 (2015).
- Yuan, H. T. *et al.* Zeeman-type spin splitting controlled by an electric field. *Nat. Phys.* **9**, 563–569 (2013).
- Ye, Y. *et al.* Electrical generation and control of the valley carriers in a monolayer transition metal dichalcogenide. *Nat. Nanotechnol.* **11**, 598–602 (2016).
- Stier, A. V., McCreary, K. M., Jonker, B. T., Kono, J. & Crooker, S. A. Exciton diamagnetic shifts and valley Zeeman effects in monolayer WS₂ and MoS₂ to 65 Tesla. *Nat. Commun.* **7**, 10643 (2016).
- Koperski, M. *et al.* Single photon emitters in exfoliated WSe₂ structures. *Nat. Nanotechnol.* **10**, 503–506 (2015).
- Sie, E. J. *et al.* Valley-selective optical Stark effect in monolayer WS₂. *Nat. Mater.* **14**, 290–294 (2015).
- Kim, J. *et al.* Ultrafast generation of pseudo-magnetic field for valley excitons in WSe₂ monolayers. *Science* **346**, 1205–1208 (2014).
- Moodera, J. S., Santos, T. S. & Nagahama, T. The phenomena of spin-filter tunnelling. *J. Phys. Condens. Mat.* **19**, 165202 (2007).
- Korenev, V. Optical orientation in ferromagnet/semiconductor hybrids. *Semiconductor Sci. Technol.* **23**, 114012 (2008).
- Wei, P. *et al.* Strong interfacial exchange field in the graphene/EuS heterostructure. *Nat. Mater.* **15**, 711–716 (2016).
- Wang, Z., Tang, C., Sachs, R., Barlas, Y. & Shi, J. Proximity-induced ferromagnetism in graphene revealed by the anomalous Hall effect. *Phys. Rev. Lett.* **114**, 016603 (2015).
- Katmis, F. *et al.* A high-temperature ferromagnetic topological insulating phase by proximity coupling. *Nature* **533**, 513–516 (2016).
- Lazic, P., Belashchenko, K. D. & Zutic, I. Effective gating and tunable magnetic proximity effects in two-dimensional heterostructure. *Phys. Rev. B* **93**, 241401 (2016).
- He, K. L. *et al.* Tightly bound excitons in monolayer WSe₂. *Phys. Rev. Lett.* **113**, 026803 (2014).
- Li, C. H. *et al.* Spin injection across (110) interfaces: Fe/GaAs(110) spin-light-emitting diodes. *Appl. Phys. Lett.* **85**, 1544–1546 (2004).

Acknowledgements

This work was supported by US National Science Foundation (MRI-1229208, DMR-1104994 and CBET-1510121), the Natural Sciences and Engineering Research Council of Canada Discovery grant RGPIN 418415-2012, the National Natural Science Foundation of China (nos 11504169, and 61575094) and the Unity Through Knowledge Fund, Contract No. 22/15. We thank Q. Niu, X. Li (University of Texas at Austin) and I. Zutic (University of Buffalo) for the insightful discussions.

Author contributions

H.Z. and A.P. conceived and designed experiments. C.Z., P.-Q.Z., P.T., K.K. and J.W. prepared and characterized the monolayer TMDCs, including WSe₂, and transferred them onto EuS substrates. P.Z., T.N., C.Z., T.S. and A.P. performed magneto-optical measurements and data analysis. Y.Y. and G.M. provided the EuS thin films. F.S. performed

magnetic measurements of EuS. R.S. and Y.C. performed the first-principle calculations. H.Z., C.Z., Y.C., R.S. G.K. and A.P. wrote the manuscript. All the authors commented on the manuscript.

Additional information

Supplementary information is available in the [online version of the paper](#). Reprints and permissions information is available online at www.nature.com/reprints. Publisher's note: Springer Nature remains neutral with regard to jurisdictional claims in published maps and institutional affiliations. Correspondence and requests for materials should be addressed to H.Z.

Competing financial interests

The authors declare no competing financial interests.

Methods

Sample preparation. Monolayer TMDCs, including WSe₂, were prepared by selenization of electron-beam evaporated ultrathin transition-metal-oxide films on sapphire substrates, similar to our previous work on MoS₂, as described in Taheri *et al.*³⁴ and Supplementary Information.

Film transfer. The as-grown monolayer TMDC films were transferred onto Si/SiO₂ and EuS substrates by modified published procedures³⁵. Briefly, monolayer WSe₂ on a sapphire substrate was covered by polymethylmethacrylate (PMMA) by spin coating. After 5 min baking at 50 °C, a water droplet was placed on the PMMA surface. The sample's edge was then poked by tweezers, and the water penetrated between the film and the substrate. After 10 min, the film completely separated from the substrate and floated on the water surface. The film was then transferred onto a Si/SiO₂ or EuS substrate, followed by 5 min baking at 80 °C. The baking of PMMA at sufficiently high temperatures stretches the PMMA, and helps to eliminate wrinkles in the TMDCs. The PMMA was removed by immersing the sample in acetone for 5 min. After repeated cleaning in acetone, the sample was then annealed in an ultrahigh vacuum chamber at 350 °C for 30 min to remove any potential adsorbates and improve the interface quality.

Optical measurements. For magnetorefectance measurements, the samples were placed on the cold finger of a continuous-flow optical cryostat operated in the 5–300 K temperature range. The cryostat was mounted on a three-axis translator with a spatial resolution of 10 μm in each direction. The *x*- and *y*-translation stages allow us to access a single TMDC crystal. The cryostat tail was positioned inside the

room temperature bore of a 7 T superconducting magnet. A collimated white-light beam was used for the reflectivity work. The incident light was focused on the sample using a microscope objective with a working distance of 34 mm. The incident beam was polarized either as LCP (σ_+) or RCP (σ_-) using a Babinet–Soleil compensator. The objective collected the reflected beam from the sample in the Faraday geometry and the light was focused onto the entrance slit of a single monochromator that uses a cooled charge-coupled device detector array.

Magnetization measurements. The field-dependent magnetization of EuS at different temperatures was measured by the VSM option of a quantum design physical property measurement system. The magnetic field was applied in the direction perpendicular to the film plane, and thus only the out-of-plane component of the magnetic moment was measured.

Data availability statement. The data that support the plots within this paper and other findings of this study are available from the corresponding author on reasonable request.

References

34. Taheri, P. *et al.* Growth mechanism of largescale MoS₂ monolayer by sulfurization of MoO₃ film. *Mater. Res. Express* **3**, 075009 (2016).
35. Gurarslan, A. *et al.* Surface-energy-assisted perfect transfer of centimeter-scale monolayer and few-layer MoS₂ films onto arbitrary substrates. *ACS Nano* **8**, 11522–11528 (2014).